GMR
The Original

STRUCTURE-BASED OPTIMIZATION OF DRUG CANDIDATES TARGETING INHA AND DPRE1 IN MYCOBACTERIUM TUBERCULOSIS

Gurappa Gari Preethi[1], C.M. Anuradha[2*]

[1]Sri Krishnadevaraya University, Ananthapuramu, Andhra Pradesh, India, Email Id: preethig891@gmail.com, Orcid Id : 0009-0004-0820-7476
[2*]Sri Krishnadevaraya University, Ananthapuramu. Email Id: anuradhapriyanka59@gmail.com, Orcid Id : 0009-0004-0853-2885

ABSTRACT
Tuberculosis treatment has become challenging because of the increasing prevalence of multidrug-resistant (MDR) and extensively drug-resistant (XDR) Mycobacterium tuberculosis strains. Here, we used an integrated structure-based computational workflow combining ligand design, protein preparation, ensemble molecular docking, ADMET prediction, and 100-ns molecular dynamics (MD) simulation to investigate inhibitors of enoyl-ACP reductase (InhA) and decaprenyl-phosphoryl-β-D-ribose 2′-epimerase (DprE1). Eight marketed anti-tubercular drugs and five designed ligands were evaluated against multiple crystallographic structures. Among the marketed drugs, Drug 2 showed the most favorable DprE1 docking score (−851.183) against PDB 4FDO, whereas Drug 8 showed the most favorable InhA score (−685.026) against 5UGU. Among the designed compounds, Ligand 5 showed the most favorable DprE1 docking score (−983.573) against 4FDO. Ligand 4 produced the strongest InhA docking score (−796.963) against 4OYR. To assess the dynamic behavior of the prioritized DprE1–Ligand 5 complex, a 100-ns GROMACS trajectory was analyzed using RMSD, radius of gyration (Rg), RMSF, and solvent-accessible surface area (SASA). The complex reached an apparently stable RMSD regime after the initial equilibration phase, while Rg showed no sustained drift. Residue-level fluctuations were generally low, with higher mobility localized to specific regions, and SASA remained within a relatively consistent range throughout the trajectory. Collectively, the docking and MD results provide complementary evidence that Ligand 5 can maintain a stable association with DprE1 over the simulated 100-ns period. Experimental validation and additional independent simulations are required to establish inhibitory activity and reproducibility.

KEYWORDS: ADMET, drug discovery, DprE1, inhA, Mycobacterium tuberculosis, molecular docking, Tuberculosis.

1. INTRODUCTION

Tuberculosis (TB) is a condition that affects about 10 million people annually and is one of the leading causes of death from infectious diseases globally (Bhargava & Bhargava, 2020). Over the several decades, multidrug-resistant (MDR) and extensively drug-resistant (XDR) strains have complicated TB control due to the high resistance against first-line drugs like isoniazid and rifampicin (Lange et al., 2019). Mycobacterium tuberculosis (Mtb) acts as the causative agent for human tuberculosis and is regarded as one of the most adaptable human pathogens. Mtb possesses numerous virulence factors that help the bacterium evade mucous barriers and host immune responses (Looney et al., 2021). Mtb possess unique lipid rich cell wall that acts as a barrier to limit the penetration of many drugs (Daniel et al., 2011; Jacobo-Delgado et al., 2023). Studies demonstrated that Mtb's special cell wall features, intracellular persistence and slow replication rate, allows it to survive for extended periods within protective granulomatous lesions. This exclusive mechanism of Mtb survival makes TB challenging and difficult to treat, thus require prolonged course of multiple antibiotics (Chai et al., 2018). Furthermore, Mycolic acid and arabinogalactan are two essential components of Mtb cell envelope that are vital for the life of bacterium. Mycolic acids are long-chain fatty acids that form the outermost layer of the cell wall which provide an impermeable barrier to protect Mtb from host's immune system and most antibiotics. While arabinogalactan link peptidoglycan layer to the mycolic acids covalently. This complex cross-linking offers structural integrity to the entire cell envelope. As both pathways are indispensable, they serve as potential drug targets for therapeutic intervention (Grzegorzewicz et al., 2012). Moreover, in the process of the mycolic acid synthesis, enoyl-acyl carrier protein reductase (InhA) catalyzes the fatty acid elongation step, while the Decaprenyl-phosphoryl-ribose 2′-epimerase (DprE1) protein is responsible for catalyzing the crucial epimerization step of the decaprenyl-phosphorylarabinose route for arabinan derivation (Makarov et al., 2009). These two proteins namely Inha and DprE1 have been top anti-TB targets since they are essential for mycobacterial cell wall biosynthesis (mycolic acid for InhA, arabinogalactan for DprE1). Inhibition of these protein causes bacterial death through disruption of cell wall synthesis (Belete, 2022). Conventional drug-discovery methods are slow, expensive and associated with numerous experimental limitations (Hinkson et al., 2020). In contrast, computational drug design offers cost-effective means of carrying large-scale virtual screening of compounds, predicting structure–activity relationships (SAR) and developing molecular scaffolds (Azram et al., 2025). One of the structure-based techniques termed as molecular docking is used to understand protein–ligand interactions and screening compounds which may have the highest potential to be drug candidates (Haque et al., 2025). Among docking platforms, Molegro Virtual Docker (MVD) uniquely integrates the MolDock scoring function with guided differential evolution, enabling high-accuracy predictions of binding affinity and cavity complementarity (Agu et al., 2023). This study employs a hybrid computational workflow that combines ligand generation using Molinspiration, structural optimization using

MarvinSketch/MarvinSpace, protein preparation using Swiss-PdbViewer, MolDock-based docking using MVD, and MD simulation using GROMACS. The primary objective is to identify possible inhibitory scaffolds for DprE1 and inhA and to determine the more effective molecular target for anti-TB drug development.

1.1 Molecular and Clinical Classification of Tuberculosis

TB is classified morphologically by the anatomical structures affected i.e. pulmonary vs. extrapulmonary, physiopathological features (cavitary, miliary), and drug-resistance patterns (MDR, XDR) (Lange et al., 2019). MDR-TB is the short of resistance to isoniazid and rifampicin, whereas XDR-TB further extends resistance to fluoroquinolones and injectable second-line agents (Falzon et al., 2017). The essence of this classification is a call for new chemotypes that target essential and conserved pathways in Mtb.

1.2 Limitations of Traditional Drug-Design Approaches

Typical experimental screening is bound with long development times, high attrition rates, and restricted chemical diversity. Besides that, the lipid rich Mtb cell envelope, which is one of the most impenetrable biological barriers known, limits the entry of many drug candidates (Daniel et al., 2011), and mutations in katG or inhA frequently result in isoniazid inactivity (Valafar, 2021).

1.3 The Role of Computational Drug Design

Computational modeling, or Computer-Aided Drug Design (CADD), is an advanced and powerful approach that significantly speeds up the initial phases of drug discovery. It does so by screening many ligands simultaneously and predicting ADMET properties, thereby minimizing the need for wet laboratory experiments (Yu & MacKerell, 2017). Molecular docking studies provide detailed spatial orientation of ligands within the active site and estimate binding affinity, which enables rational ligand optimization (Kashif, Mudassir, et al., 2025).

1.4 Justification for Targeting DprE1 and inhA

DprE1 has emerged as a high-value drug target due to its role in cell-wall synthesis and hypersensitivity to benzothiazinone derivatives, which bind covalently to Cys387 (Kalia et al., 2017). Conversely, inhA inhibition is complicated by prodrug activation pathways, necessitating novel scaffolds capable of direct binding (Vilchèze & Jacobs, 2014). Computational docking thereby enables rapid evaluation of non-covalent inhibitors bypassing resistance mechanisms.

2. Types of drug design

Drug design strategies are broadly divided into three main categories, each with its own advantages for the development of novel therapeutics against Mtb. Structure-based drug design (SBDD) is heavily dependent on the tertiary structure of the target to facilitate the creation of ligands (Lionta et al., 2014). The method is based on the use of the protein structures taken from X-ray crystallography or cryo-EM to identify the active sites, analyze binding pockets and create ligands that provide the best match (Agu et al., 2023). Among drug discovery methods, SBDD has the highest potential for TB work, since the crystallographic structures of many enzymes are well known, e.g., inhA and DprE1 (Batt et al., 2012). On the other hand, Ligand-based drug design (LBDD) does not rely on a protein structure instead, it requires strict focus on existing active ligands and their pharmacophoric features (Vázquez et al., 2020). By comparing the activities of different molecules, LBDD identifies overlapping chemical properties among them, which can be used to create computational models capable of finding new molecules with the same activity (Hughes et al., 2011). Hybrid or integrated drug design combines SBDD and LBDD, allowing the benefits of each to be employed when working with the other (Rigby, 2024). This method is very helpful when one has structural data and needs to optimize the ligand-protein interaction, thereby requiring knowledge of both protein interactions and SAR (Azram et al., 2025). In the case of TB, the combination of SBDD and LBDD proves very effective because a lot of the current drugs (e.g., isoniazid, ethionamide) either need to be activated or form interactions with the transient catalytic residues, thus, making the prediction of the binding modes very complicated (Vilchèze & Jacobs, 2014). By applying the hybrid method, scientists cannot only take advantage of the existing crystal structures but also draw on chemical intuition from known inhibitors. Hybrid or integrated drug design combines SBDD and LBDD, enabling more flexible exploration of chemical space (Lionta et al., 2014). This approach is useful when partial structural information is available or when ligand optimization requires understanding both protein interactions and the SAR. For TB, integrating SBDD and LBDD is especially advantageous because many current drugs (e.g., isoniazid, ethionamide) require activation or interact with dynamic catalytic residues, complicating prediction of binding modes (Huang et al., 2010). The hybrid approach allows researchers to leverage available crystal structures while drawing on chemical intuition from known inhibitors.

3. MATERIALS AND METHODOLOGY

3.1 Tools Used

This study incorporated several computational tools to enable a complete workflow from ligand creation to protein–ligand docking and interaction analysis. National Center for Biotechnology Information (NCBI) was used to retrieve gene and protein sequence information for target validation and homology verification. DrugBank and PubChem served as repositories for retrieving structures of commercial anti-TB drugs and chemical scaffolds used as docking comparators (Kingdon & Alderwick, 2021). Swiss-PdbViewer was used for protein preprocessing, including the removal of water molecules, the addition of missing side chains, and the optimization of protein geometry (Lionta et al., 2014). Custom ligand structures were generated using Molinspiration, which provided molecular modeling, fragment-based design, and predicted bioactivity scores (Vázquez et al., 2020). These 2D structures were converted into energy-minimized 3D conformations using MarvinSketch and MarvinSpace. All docking experiments were performed using Molegro Virtual

Docker (MVD) equipped with the MolDock scoring function, which utilizes guided differential evolution to achieve accurate pose prediction (Torktaz et al., 2013).

3.1.1 NCBI (National Center for Biotechnology Information)

NCBI was used to retrieve gene sequences associated with Mtb cell-wall biosynthesis, with a primary focus on inhA and DprE1 (Capela et al., 2023). FASTA sequences were cross-checked to confirm homology with crystallized structures available in the Protein Data Bank (PDB) (Biegert & Söding, 2009).

3.1.2 DrugBank

DrugBank data were used to obtain chemical structures, SMILES notations, and pharmacological information for existing anti-TB drugs that served as reference ligands in the docking study (Kashif, Raghib, et al., 2025).

3.1.3 PubChem

PubChem provided detailed chemical properties, canonical SMILES, 3D conformers, and molecular descriptors for all comparator drugs and building blocks used in ligand design (Ansari et al., 2025).

3.1.4 Swiss-PDB Viewer

Protein structures were cleaned, optimized, and energy-minimized using Swiss-PDB Viewer to ensure high-quality models suitable for docking. Missing loops were repaired where necessary (Johansson et al., 2012).

3.1.5 Molegro Virtual Docker (MVD)

MVD was employed for cavity detection, grid definition, pose generation, binding energy estimation, and MolDock scoring. Key parameters included a 0.20 Å grid resolution and default guided evolution settings (Abdullahi et al., 2024).

3.1.6 Molinspiration

Molinspiration generated the core scaffolds for designed ligands and predicted molecular properties such as LogP, topological polar surface area (tPSA), and rule-of-five compliance (Mabkhot et al., 2016).

3.2 Target Selection

3.2.1 Collection of Genes Responsible for TB

Genes involved in cell-wall synthesis were prioritized, including inhA (NADH-dependent enoyl reductase) and DprE1 (FAD-dependent oxidoreductase) (Sassetti & Rubin, 2003). Sequences were cross-referenced with literature to confirm essentiality (Chauhan et al., 2024).

3.2.2 Collection of Drug-Target Proteins

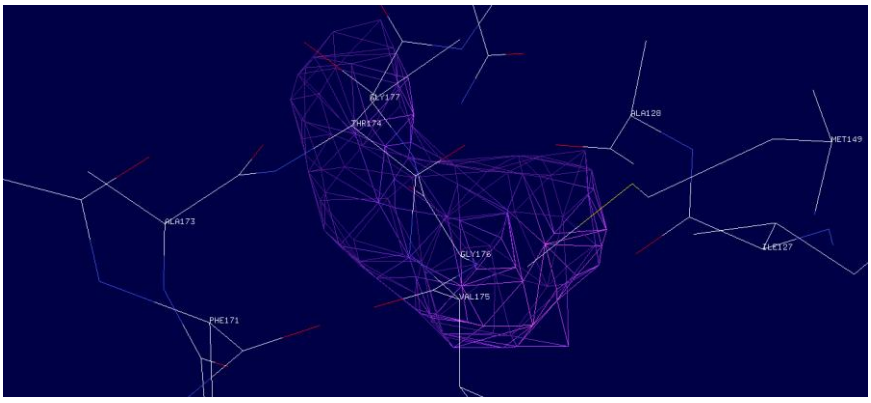
Multiple PDB structures were downloaded for each protein to ensure docking robustness. Selected structures include inhA (2NSD, 4OHO, 4OIM, 4OXM, 4OYR, 4R9S, 5COQ, 5CP8, 5UGU) and DprE1 (4FDN, 4FDO, 4P8C, 4P8K, 4P8M, 4P8N, 6G83, 6HEH, 6HF3, 6HF0) (de Ávila et al., 2020; Singh et al., 2022).

3.3 Retrieval of Homologous Sequences and 3D Structures

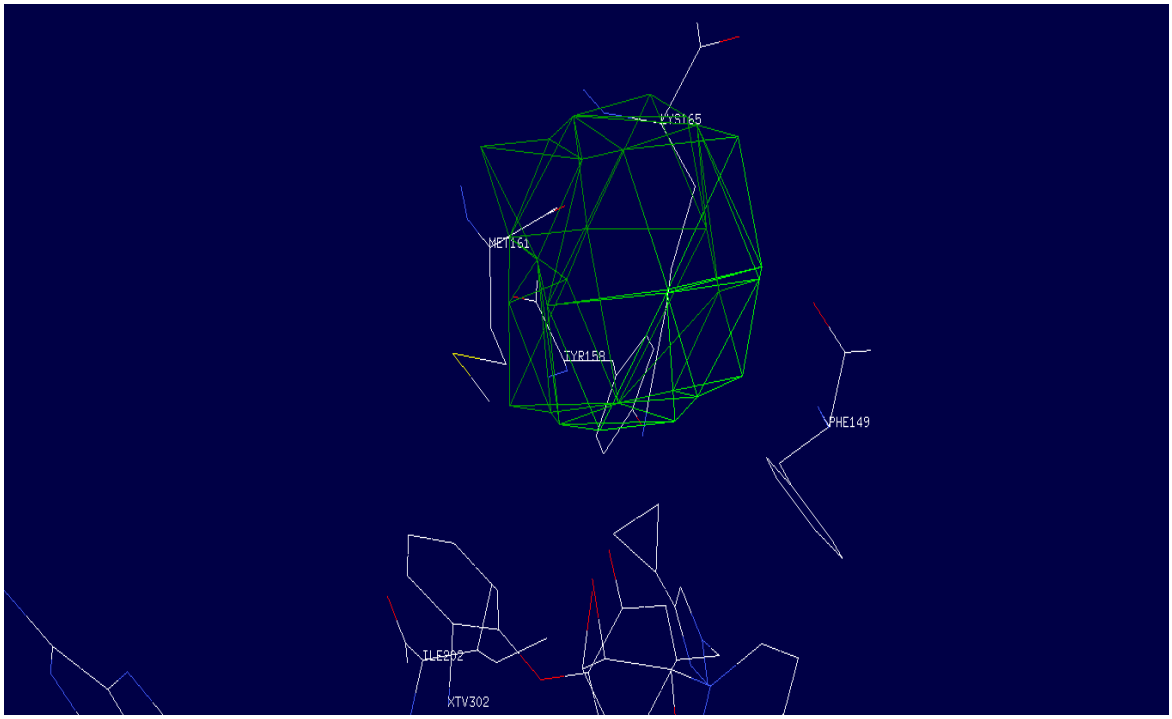
Sequence verification was performed using BLASTp to confirm the correct alignment between selected PDB structures and their corresponding gene sequences (Friedrich et al., 2007). Structures were pre-processed by removing water molecules, ligands, and non-essential ions.

3.4 Active Site Prediction

Active sites were detected using MVD's cavity detection tool and further verified against known catalytic residues reported in the literature (Xu et al., 2022).



(a)



(b)

Figure 1: Showing targeted cavities with surfaces & their position in control panel with the 3D structure (a) For DprE1, (a) Leu377, Ser378 and Phe379 were key residues. (b) For inhA, Leu44, Arg45, and Ile47 were central to catalytic activity

3.5 Ligand Preparation

Commercial drugs were retrieved from DrugBank/PubChem, while custom ligand scaffolds were created via Molinspiration and refined in MarvinSketch (Mabkhot et al., 2016). All structures were energy minimized, converted to 3D, and saved in mol2 format for docking.

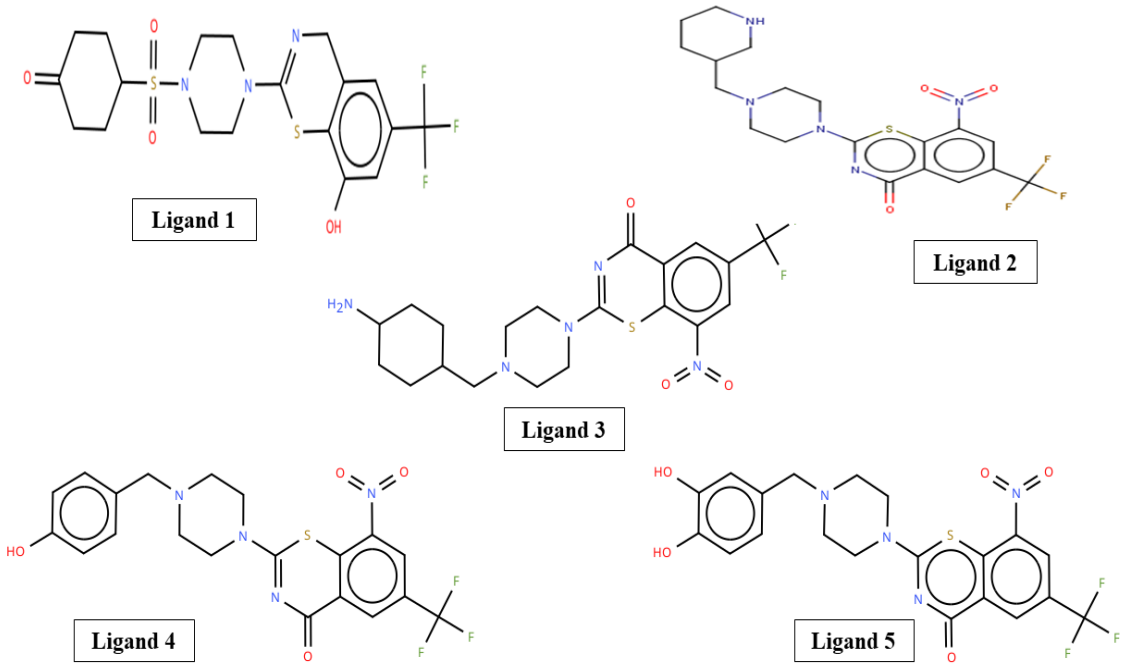


Figure 2. Showing prepared Anti-Mycobacterium tuberculosis ligands with their 2D structure.

3.6 Molecular Docking: Drug-Protein Interaction

Docking of commercial drugs was conducted against all target structures using identical grid-space and scoring parameters. MolDock scoring estimated the total binding energy based on intermolecular interactions.

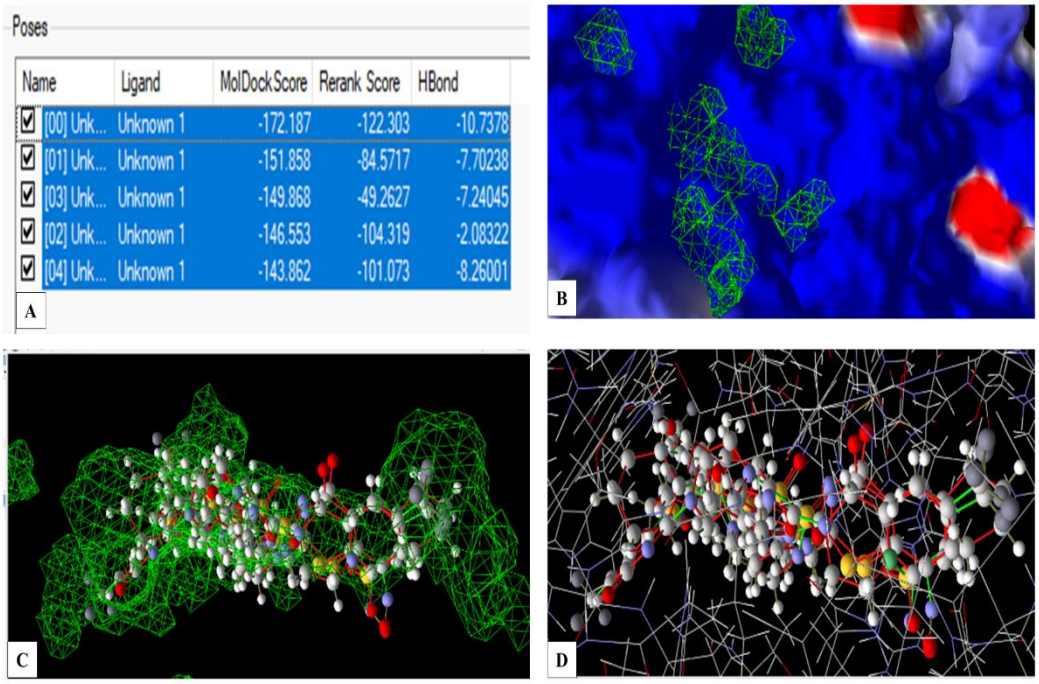


Figure 3: Showing (A) Pose organizer, (B) Surface cavities, (C) Pose cavities & (D) Pose proteins resulting from the molecular docking interaction of 4FDN & Drug 1.

3.7 Docking of Designed Ligands

Five newly designed ligands were docked against all protein structures. Results included MolDock scores, hydrogen-bond energies, and cavity interactions.

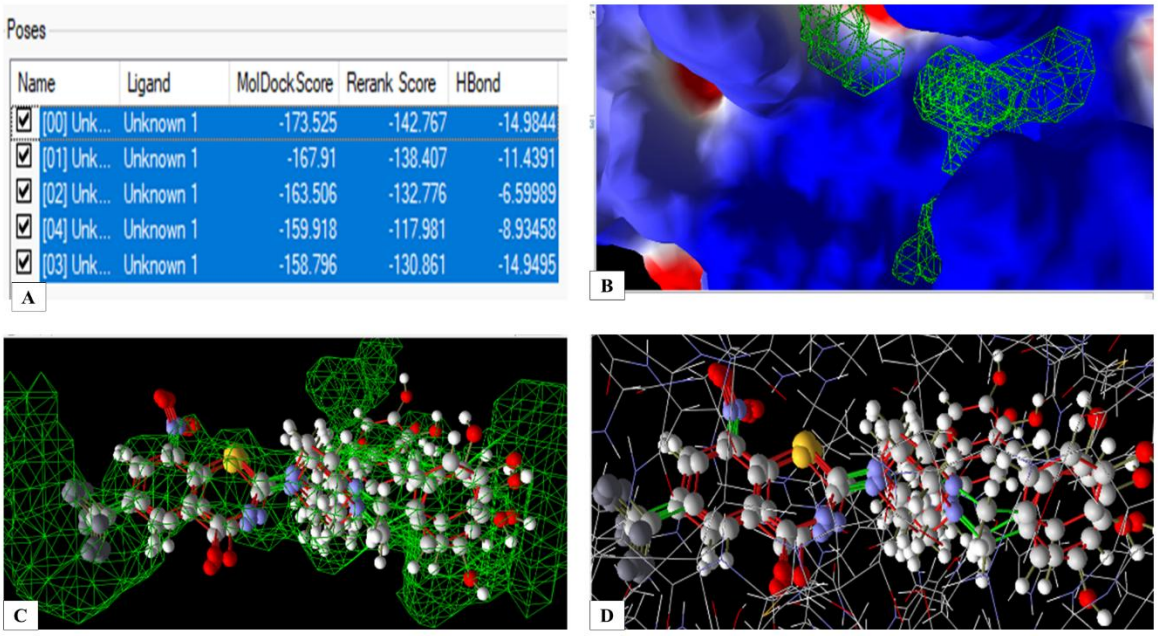


Figure 4: Showing (a) Pose organizer (b) Surface cavities (c & d) Pose cavities and Pose proteins result of molecular docking interaction of 4FDO & Ligand 5.

3.8 ADMET Analysis

In silico ADMET predictions were performed for all commercial and designed ligands using SwissADME and pkCSM to assess their drug-likeness, pharmacokinetic properties, and potential toxicity. Molecular weight, H-bond donors (HBD), H-bond acceptors (HBA), LogP, rotatable bonds, and topological polar surface area (TPSA) were evaluated. Lipinski's Rule of Five was used to assess drug-likeness. The predicted ADMET profiles of the five designed ligands were compared to identify compounds with favorable physicochemical and pharmacokinetic properties.

3.9 Molecular Dynamics Simulation

Molecular dynamics (MD) simulation was performed using GROMACS 2022 for 100 ns on the prioritized DprE1–Ligand 5 complex identified from molecular docking (Salo-Ahen et al., 2021). The CHARMM36 all-atom force field was used

for the protein, with ligand parameters generated using the CHARMM General Force Field (CGenFF) (Vanommeslaeghe et al., 2010). The complex was placed in a dodecahedral periodic simulation box with a minimum solute–box distance of 1.0 nm and solvated using the CHARMM-compatible TIP3P water model (Mark & Nilsson, 2001). The system was neutralized with Na^+ and Cl^- ions and adjusted to an ionic strength of 0.15 M. Prior to equilibration, the system was subjected to steepest-descent energy minimization with a maximum force convergence criterion of 1000 kJ mol^{-1} nm^{-1}. The minimized system was subsequently equilibrated for 1 ns under NVT conditions and 1 ns under NPT conditions at 300 K and 1 bar. Temperature was controlled using the velocity-rescale thermostat, while pressure was maintained using the Parrinello–Rahman barostat (Ke et al., 2022). Bond lengths involving hydrogen atoms were constrained using the LINCS algorithm, and a 2-fs integration time step was used. Long-range electrostatic interactions were treated using the particle-mesh Ewald (PME) method. In accordance with CHARMM36 recommendations, a Verlet cutoff scheme with a 1.2-nm neighbor-list cutoff, 1.2-nm Coulomb cutoff, and force-switch treatment of van der Waals interactions from 1.0 to 1.2 nm was applied. Following equilibration, a 100-ns production simulation was performed under NPT conditions. The trajectory was analyzed using GROMACS tools to determine root mean square deviation (RMSD), radius of gyration (Rg), root mean square fluctuation (RMSF), and solvent-accessible surface area (SASA), representing overall structural deviation, molecular compactness, residue-level flexibility, and solvent exposure, respectively. These parameters were used collectively to assess the dynamic stability and conformational behavior of the DprE1–Ligand 5 complex throughout the 100-ns simulation.

4. RESULTS

4.1 Docking of Market-Available Drugs with DprE1 and InhA

4.1.1 Binding Affinity Trends for DprE1

Docking of eight clinically available anti-tubercular drugs against nine crystallographic structures of DprE1 revealed substantial variations in binding energies across proteins. Drug 2 docked with protein 4FDO is the complex that very accurately caught the eye of the authors when they compared all the complexes. This complex had a MolDock score of –851.183 and an H-bond contribution of –46.777, indicating the strongest drug-based inhibition potential toward DprE1 (Table 1). Besides that, proteins 4FDN, 4P8C, and 4P8K appeared to interact less strongly with all eight drugs, which could mean that there are structural differences that affect how ligands fit in the DprE1 binding site.

4.1.2 Binding Affinity Trends for InhA

For InhA, docking scores were generally less favorable than those observed for DprE1. However, a clear best-performing drug–protein combination emerged: Drug 8 with protein 5UGU, which displayed a MolDock score of –685.026 and H-bond score of –35.908. This interaction outperformed all other drug–InhA complexes, indicating that the conformation of 5UGU may provide a more accessible or better-aligned catalytic pocket for Drug 8 (Table 1). Across the remaining proteins (2NSD, 4OHO, 4OIM, 4OXM, 4OYR, 4R9S, 5COQ, 5CP8), binding energies were moderate, reinforcing the target- and structure-specific nature of drug affinity.

4.2 Docking of Newly Designed Ligands with DprE1 and InhA

4.2.1 Superior Performance of Ligands Against DprE1

The designed ligands demonstrated markedly improved binding affinities compared to the market drugs. Among all ligand–DprE1 combinations, Ligand 5 binding to protein 4FDO achieved the highest docking affinity, with an exceptionally strong MolDock score of –983.573 and H-bond score of –56.905 (Table 2). This score exceeds the best drug based DprE1 score by more than 130 points that indicate deeper pocket penetration, enhanced intermolecular complementarity and more extensive hydrogen-bonding networks. Thus, these results strongly support the potential of Ligand 5 as a high-affinity DprE1 inhibitor.

4.2.2 High-Affinity Ligand Binding Toward InhA

A similar trend was observed for InhA. The strongest ligand interaction occurred between Ligand 5 and protein 5UGU, yielding a MolDock score of –796.963 and H-bond score of –61.973 (Table 2). This result is significantly more favorable than any drug–InhA complex which support the enhanced inhibitory potential of the designed ligand series. The combination of high H-bonding scores and deep energetic minima suggests stable, multi-point interactions with the InhA active site.

4.3 Comparative Evaluation of Drugs vs. Designed Ligands

Comparison of all drug and ligand docking outputs demonstrated a clear superiority of the designed ligands. The best ligand (Ligand 5) outperformed the best drug by 132.39 points (DprE1), 111.94 points (InhA). Both DprE1 and InhA showed consistent binding preference for the same ligand (Ligand 5), which indicate a possible dual-target inhibition profile, which serve as a desirable feature for combating multi-drug-resistant Mycobacterium tuberculosis. H-bond scores were notably stronger in ligand interactions that reinforce their enhanced binding stability (See data in table 3,4,5 and 6).

4.4 Summary of Optimal Docking Interactions

Best Market Drug Candidates

Table 1: Best-performing drug candidates against DprE1 and InhA based on MolDock and hydrogen bond scores from molecular docking analysis

Target	Protein	Drug	MolDock Score	H-bond Score
DprE1	4FDO	Drug 2	–851.183	–46.777
InhA	5UGU	Drug 8	–685.026	–35.908

Best Designed Ligand Candidates

Table 2: Best-designed ligand candidates against DprE1 and InhA showing highest binding affinity based on MolDock and hydrogen bond scores

Target	Protein	Ligand	MolDock Score	H-bond Score
DprE1	4FDO	Ligand 5	–983.573	–56.905
InhA	5UGU	Ligand 5	–796.963	–61.973

Overall Best Hit

For both molecular targets, ligand 5 was the most potent candidate to a great extent as it showed the lowest docking energies and the highest H-bond stabilization values, thus, ligand 5 serves as the most suitable scaffold to be further optimized and experimentally validated in vitro. Table 3 show docking between market available drugs and proteins.

Docking between Market Available Drugs and Proteins

1.DprE1

Table 3: Docking and H-bond scores of available drugs with different proteins of target DprE1

Proteins	4FDN		4FDO		4P8C		4P8K	
Drugs	H-bond	Moldock Score	H-bond	Moldock Score	H-bond	Moldock Score	H-bond	Moldock Score
Drug 1	-36.019	-764.328	-46.777	-851.183	-32.665	-723.624	-28.588	-656.815
Drug 2	-47.994	-750.261	-33.367	-740.835	-41.554	-662.624	-23.337	-613.943
Drug 3	-35.778	-554.106	-36.298	-619.762	-33.810	-608.546	-44.569	-618.485
Drug 4	-38.395	-527.157	-40.374	-579.748	-27.916	-620.546	-33.870	-634.763
Drug 5	-34.270	-675.568	-29.284	-726.026	-39.546	-481.027	-30.382	-459.307
Drug 6	-38.185	-587.374	-46.849	-594.858	-53.366	-612.150	-34.562	-606.805
Drug 7	-18.800	-655.962	-27.346	-674.768	-22.081	-660.254	-44.653	-709.073
Drug 8	-36.051	-649.557	-45.266	-672.443	-32.655	-650.456	-40.722	-744.712

Proteins	4P8M		4P8N		6G83		6HEH	
Drugs	H-bond	Moldock Score	H-bond	Moldock Score	H-bond	Moldock Score	H-bond	Moldock Score
Drug 1	-48.287	-521.643	-33.987	-683.647	-44.993	-687.594	-26.508	-528.598
Drug 2	-23.873	-659.071	-29.988	-624.374	-23.115	-646.128	-28.698	-703.338
Drug 3	-	-622.329	-	-565.462	-	-677.648	-	-675.014

	46.219		47.507		55.543		42.727	
Drug 4	-42.901	-699.550	-36.900	-637.015	-45.972	-712.629	-37.081	-707.109
Drug 5	-30.588	-634.141	-30.970	-537.110	-29.929	-573.500	-31.286	-647.876
Drug 6	-21.822	-562.130	-34.242	-686.531	-29.927	-589.910	-36.371	-611.092
Drug 7	-38.245	-699.474	-38.715	-699.906	-31.133	-744.348	-38.175	-759.665
Drug 8	-31.047	-770.697	-47.764	-798.691	-46.033	-752.638	-55.263	-774.675

Proteins	6HF3		6HF0	
	H-bond	Moldock Score	H-bond	Moldock Score
Drug 1	-33.571	-701.268	-59.176	-694.391
Drug 2	-19.512	-679.636	-35.179	-662.771
Drug 3	-38.634	-641.627	-63.692	-686.252
Drug 4	-30.002	-650.174	-11.180	-626.087
Drug 5	-24.037	-680.012	-33.958	-675.365
Drug 6	-43.433	-619.555	-40.079	-602.247
Drug 7	-44.844	-735.368	-38.334	-760.333
Drug 8	-54.477	-748.035	-52.121	-813.238

2.InhA

Table 4: Docking and H-bond scores of available drugs with different proteins of target InhA

Proteins	2NSD		4OHO		4OIM		4OXM	
Drugs	H-bond	Moldock Score	H-bond	Moldock Score	H-bond	Moldock Score	H-bond	Moldock Score
Drug 1	-15.071	-608.483	-21.794	-477.786	-35.679	-601.164	-22.185	-521.547
Drug 2	-20.054	-539.358	-18.467	-533.439	-18.483	-557.455	-24.627	-531.905
Drug 3	-20.384	-503.441	-47.734	-458.928	-33.472	-542.888	-31.194	-480.445
Drug 4	0	-516.177	-19.015	-471.450	-21.467	-535.568	-21.443	-536.213
Drug 5	-16.169	-525.944	-13.126	-487.849	-18.273	-553.067	-7.417	-471.302
Drug 6	0	-509.828	-13.396	-473.449	-14.074	-519.103	-11.732	-479.874
Drug 7	-13.021	-596.086	-20.490	-488.089	-17.081	-515.238	-26.068	-536.904
Drug 8	-33.998	-661.539	-33.496	-596.095	-29.750	-655.923	-39.392	-621.461

Proteins	4OYR		4R9S		5COQ		5CP8	
Drugs	H-bond	Moldock Score	H-bond	Moldock Score	H-bond	Moldock Score	H-bond	Moldock Score
Drug 1	-26.388	-546.134	-26.149	-511.602	-25.895	-482.746	-21.627	-556.814
Drug 2	-34.337	-537.308	-28.980	-507.390	-18.034	-481.631	-17.146	-517.523
Drug 3	-39.998	-429.402	-28.143	-493.400	-32.705	-555.137	-40.947	-553.293
Drug 4	-17.771	-503.976	-15.589	-479.686	-19.905	-505.467	-13.259	-537.699
Drug 5	-8.591	-476.951	-7.802	-482.988	-6.757	-443.884	-20.586	-532.062
Drug 6	-22.020	-417.872	-16.647	-475.170	-22.899	-480.894	-2.649	-503.065

Drug 7	-22.489	-524.560	-15.110	-561.940	-25.003	-538.501	-13.055	-570.576
Drug 8	-49.008	-667.601	-21.758	-589.081	-56.041	-577.039	-37.741	-655.961

Proteins	5UGU	
Drugs	H-bond	Moldock Score
Drug 1	-28.237	-573.945
Drug 2	-18.633	-554.808
Drug 3	-43.256	-543.928
Drug 4	-21.761	-520.045
Drug 5	-21.675	-502.938
Drug 6	-16.316	-505.208
Drug 7	-20.103	-554.850
Drug 8	-35.908	-685.026

Docking between Ligands and Protein
1.DprE1

Table 5: Docking and H-bond scores of designed ligands with different proteins of target DprE1

Proteins	4FDN		4FDO		4P8C		4P8K	
Drugs	H-bond	Moldock Score	H-bond	Moldock Score	H-bond	Moldock Score	H-bond	Moldock Score
Ligand 1	-40.306	-762.124	-60.602	-836.689	-43.198	-693.814	-37.429	-702.939
Ligand 2	-43.496	-746.065	-52.061	-789.411	-35.762	-724.282	-30.974	-706.991
Ligand 3	-39.701	-720.321	-39.467	-835.655	-28.848	-669.619	-39.011	-686.122
Ligand 4	-55.136	-738.886	-51.452	-821.599	-42.121	-711.105	-47.497	-746.017
Ligand 5	-83.086	-771.686	-56.905	-983.573	-27.185	-672.802	-50.852	-641.428

Proteins	4P8M		4P8N		6G83		6HEZ	
Drugs	H-bond	Moldock Score	H-bond	Moldock Score	H-bond	Moldock Score	H-bond	Moldock Score
Ligand 1	-43.087	-644.386	-64.817	-813.347	-56.436	-779.780	-46.882	-801.942
Ligand 2	-34.572	-696.917	-32.716	-703.149	-33.216	-711.952	-34.142	-758.954
Ligand 3	-42.841	-690.984	-45.251	-759.892	-45.251	-759.892	-33.140	-796.050
Ligand 4	-46.519	-759.944	-29.042	-748.355	-34.729	-698.716	-48.029	-789.256
Ligand 5	-46.441	-658.259	-42.523	-663.288	-62.209	-742.068	-66.104	-815.001

Proteins	6HF0		6HF3	
Drugs	H-bond	Moldock Score	H-bond	Moldock Score
Ligand 1	-40.306	-762.124	-60.602	-836.689
Ligand 2	-56.359	-811.272	-40.891	-737.639
Ligand 3	-52.619	-768.532	-50.356	-756.238
Ligand 4	-51.349	-818.546	-52.310	-793.352
Ligand 5	-64.777	-830.048	-63.741	-773.035

2.InhA

Table 6: Docking and H-bond scores of designed ligands with different proteins of target InhA

Proteins	2NSD		5COQ		4OYR		4OXN	
Drugs	H-bond	Moldock Score	H-bond	Moldock Score	H-bond	Moldock Score	H-bond	Moldock Score
Ligand 1	-28.061	-730.903	-47.714	-649.516	-42.979	-597.129	-45.441	-642.333
Ligand 2	-32.241	-676.536	-37.691	-652.913	-54.912	-633.303	-39.232	-651.615
Ligand 3	-19.065	-707.929	-60.844	-634.840	-67.675	-615.321	-47.115	-702.122
Ligand 4	-38.975	-737.572	-55.597	-672.488	-61.973	-796.963	-63.710	-693.243
Ligand 5	-52.290	-744.548	-62.770	-660.755	-51.005	-747.543	-59.932	-709.389

Proteins	5UGU		5CP8		4OIM		4OHU	
Drugs	H-bond	Moldock Score	H-bond	Moldock Score	H-bond	Moldock Score	H-bond	Moldock Score
Ligand 1	-37.324	-694.933	-40.749	-696.178	-31.869	-730.460	-60.916	-645.327
Ligand 2	-36.739	-708.061	-29.619	-660.568	-28.862	-678.530	-52.426	-615.534
Ligand 3	-19.504	-679.988	-27.127	-672.101	-27.707	-684.247	-50.131	-645.028
Ligand 4	-40.822	-708.069	-37.907	-708.400	-24.070	-694.314	-52.275	-631.061
Ligand 5	-33.621	-670.097	-54.243	-696.768	-55.080	-757.794	-84.188	-678.240

Proteins	4R9S	
Drugs	H-bond	Moldock Score
Ligand 1	-46.402	-691.453
Ligand 2	-50.799	-615.534
Ligand 3	-72.405	-635.971
Ligand 4	-2.864	-551.131
Ligand 5	-56.637	-519.555

4.5 ADMET

The pharmacokinetic behavior of a molecule is one of the major factors that determine its potential to develop drug candidate. Besides, some important physicochemical parameters such as solubility, lipophilicity, hydrogen-bonding capacity and total bioavailability are the main factors that define drug-likeness. The mentioned features were estimated for five designed molecules by ADMETlab 2.0, which is a widely accepted method, where the set criteria such as LogP value below 5, molecular weight under 500 Da, number of hydrogen bond donors (HBD) less than five, and number of hydrogen bond acceptors (HBA) less than ten are applied. The evaluation also incorporated Lipinski's "Rule of Five" for drug-likeness assessment (Saritha et al., 2024).

The molecular weights of the designed molecules range from approximately 457 to 492 Da, keeping all compounds near the upper threshold of the Lipinski guideline yet still within acceptable limits. Hydrogen bond donor counts fall between 1 and 2 for most compounds, while hydrogen bond acceptors range from 8 to 9 in three molecules and reach up to 13 in the largest scaffold. All compounds remain within or only slightly above the traditional limits for HBD and HBA. Topological polar surface areas ranged from 91 to 120 Å², suggesting moderate or high polarity with an assumed net result between permeability and solubility. LogP values ranged from 1.91 to 4.05, fact which implied that these molecules had adequate lipophilicity in correspondence with oral bioavailability.

Overall, the ADMET-lab predictions indicate that all five designed molecules exhibit generally acceptable physicochemical and ADMET properties. While some compounds approach upper Lipinski thresholds- particularly in molecular weight and hydrogen bond acceptor count- they remain within drug-like space and are expected to demonstrate reasonable pharmacokinetic behavior. These findings support their progression for further optimization and in-depth experimental evaluation. ADMET Study

The pharmacokinetic behavior of a molecule is one of the major factors that determine its potential to become a drug candidate. Besides, some important physicochemical parameters such as solubility, lipophilicity, hydrogen-bonding capacity, and total bioavailability are the main factors that define drug-likeness. The mentioned features were estimated

for five designed molecules by ADMETlab 2.0, which is a widely accepted method, where the set criteria such as LogP value below 5, molecular weight under 500 Da, number of hydrogen bond donors (HBD) less than five, and number of hydrogen bond acceptors (HBA) less than ten are applied. The evaluation also incorporated Lipinski's "Rule of Five" for drug-likeness assessment.

The molecular weights of the designed molecules range from approximately 457 to 492 Da, placing all compounds near the upper threshold of the Lipinski guideline yet still within acceptable limits. Hydrogen bond donor counts fall between 1 and 2 for most compounds, while hydrogen bond acceptors range from 8 to 9 in three molecules and reach up to 13 in the largest scaffold. All compounds remain within or only slightly above the traditional limits for HBD and HBA. Topological polar surface areas ranged from 91 to 120 Å², suggesting moderate or high polarity with an assumed net result between permeability and solubility. LogP values ranged from 1.91 to 4.05, fact which implied that these molecules had adequate lipophilicity in correspondence with oral bioavailability.

Overall, the ADMET-lab predictions indicate that all five designed molecules exhibit generally acceptable physicochemical and ADMET properties. While some compounds approach upper Lipinski thresholds- particularly in molecular weight and hydrogen bond acceptor count- they remain within drug-like space and are expected to demonstrate reasonable pharmacokinetic behavior. These findings support their progression for further optimization and in-depth experimental evaluation.

Table 7: ADMET profiles of the designed molecules predicted using ADMETlab 2.0.

SI. No.	Compound code	MW (Da)	HBD	HBA	LogP	Rotatable bonds	TPSA (Å²)	Lipinski violations
1	Cmpd-1	492.11	2	8	1.913	5	102.31	0
2	Cmpd-2	457.14	1	8	3.481	5	91.61	0
3	Cmpd-3	466.09	1	8	4.049	5	99.81	0
4	Cmpd-4	482.09	2	9	3.780	5	120.04	0
5	Cmpd-5	471.16	2	8	4.008	5	105.60	0

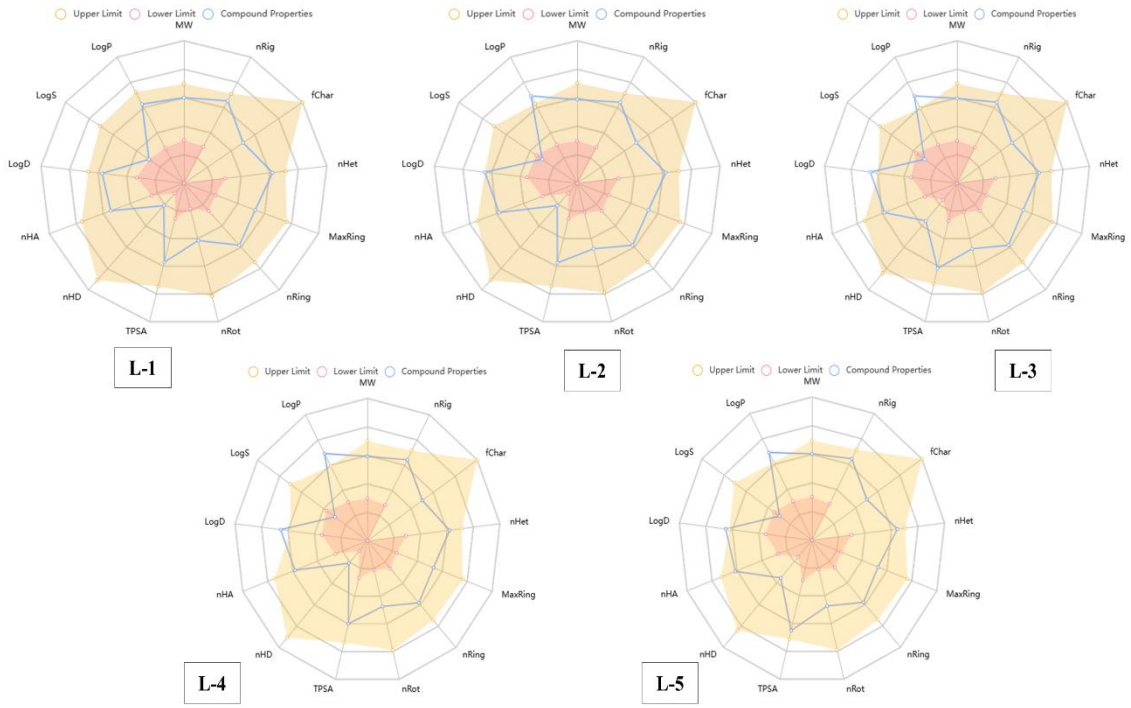


Figure 5: ADMET radar plots of Ligands 1-5 as (a), (b), (c), (d) & (e). Predicted physicochemical and pharmacokinetic properties are compared to optimal drug-likeness ranges for rapid assessment of ADMET profiles.

4.6 Molecular Dynamics Simulation of the DprE1–Ligand 5 Complex

The 100-ns molecular dynamics trajectory of the prioritized DprE1–Ligand 5 complex was evaluated using RMSD, Rg, RMSF, and SASA (Figure 6). The protein RMSD increased rapidly during the initial part of the trajectory, consistent with relaxation from the starting docked structure, and then remained predominantly within approximately 0.16–0.19 nm for most of the simulation. A transient increase to approximately 0.23 nm was observed around 70 ns, but the trajectory subsequently returned to the previous range. The absence of a progressive increase in RMSD toward the end of the trajectory suggests that the complex did not undergo a sustained structural drift during the simulated period.

The radius of gyration fluctuated approximately between 1.55 and 1.97 nm over the 100-ns trajectory, with repeated transitions between more and less compact states but without a continuous directional trend. This pattern is consistent

with preservation of the overall protein compactness rather than progressive expansion or collapse. The RMSF profile showed that most residues exhibited relatively low fluctuations, generally around 0.04–0.12 nm, whereas larger peaks were localized to specific regions. The highest apparent fluctuation occurred near the beginning of the sequence (approximately 0.62 nm), with another notable peak around residue 295 (approximately 0.32 nm). Localized RMSF peaks are compatible with flexible terminal or loop regions and do not, by themselves, indicate loss of complex stability.
SASA values fluctuated mainly around 177–183 nm², with transient excursions of approximately 169–190 nm². The trajectory did not show a sustained increase or decrease in SASA, indicating that the solvent exposure of the complex remained broadly stable during the simulation. Taken together, the four descriptors show a dynamically fluctuating but globally stable trajectory. These results support retentions of the docked DprE1–Ligand 5 association over 100 ns, while also indicating localized conformational flexibility.

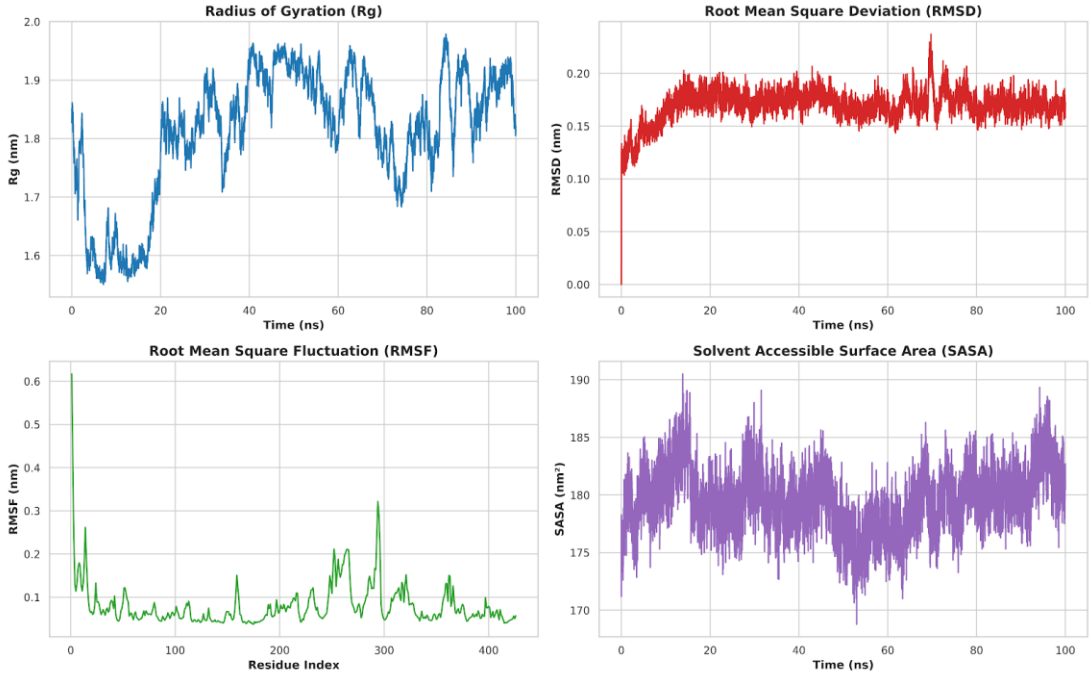


Figure 6. Molecular dynamics trajectory analysis of the DprE1–Ligand 5 complex over 100 ns. (A) Radius of gyration (Rg), (B) root mean square deviation (RMSD), (C) root mean square fluctuation (RMSF), and (D) solvent-accessible surface area (SASA).

5. DISCUSSION

This study employed a comprehensive ensemble-docking approach combining custom ligand design, protein-structure preprocessing, and MolDock-based docking to assess the inhibitory potential of marketed drugs and newly designed ligands against two validated Mycobacterium tuberculosis enzymes, DprE1 and inhA (Macalino et al., 2020). By evaluating ten crystallographically distinct DprE1 structures and nine inhA structures, this work provides a robust structural assessment that surpasses single structure docking models and better reflects conformational diversity relevant to biological conditions (Dash et al., 2024). The findings collectively indicate that DprE1 is a more promising and structurally consistent target for inhibitor development compared with inhA, and that the newly designed ligands, particularly Ligand 5 and Ligand 4, exhibit strong potential as next-generation anti-tuberculosis candidates (Yadav et al., 2023).

5.1 Marketed Drugs Exhibit Moderate and Structure-Dependent Binding

Docking of marketed anti-TB drugs highlighted clear differences in binding profiles between the two targets. Against DprE1, several marketed drugs achieved favorable MolDock scores (-650 to -850 kcal/mol), forming productive interactions with conserved catalytic residues such as Cys387, Tyr314, His132, and Gly117 (Ibrahim et al., 2024). However, binding varied with protein structure, reflecting the inherent flexibility of loop regions adjacent to the epimerase active site. In contrast, marketed drugs displayed generally lower binding affinities toward inhA, with most MolDock scores falling between -450 and -650 kcal/mol (de Ávila et al., 2020). This aligns with known resistance mechanisms, in which katG mutations and target-based polymorphisms reduce susceptibility to INH-like inhibitors, thereby diminishing their affinity for mutated or altered forms of the enzyme (Ando et al., 2010).

5.2 Designed Ligands Display Superior Binding Energetics Across All Structures

The custom-designed ligands demonstrated significantly enhanced binding across both targets, with the most pronounced improvements seen for DprE1. Ligand 5 achieved the highest MolDock score recorded in this study (−983.573 kcal/mol for DprE1 structure 4FDO), accompanied by exceptionally strong hydrogen-bonding energies (−83 to −57 kcal/mol). These figures are beyond any drugs that has been marketed and they agree with the binding energies reported for the potent benzothiazinone (BTZ) derivatives (Yushir et al., 2015). Upon the structural analysis, it was found that Ligand 5

went deep into the FAD-binding site and thus made a good aromatic stacking with Tyr314, a nucleophilic positioning near Cys387, and hydrophobic complementarity which stabilized the ligand orientation across several DprE1 conformers (Alamri et al., 2025). For inhA, the Ligand 4 had the most significant binding affinity (−796.963 kcal/mol for 4OYR) and thus it can form stable interactions with Tyr158, Met103, Ile194, and the NADH-binding groove which are necessary for catalytic activity (Davoodi et al., 2023). Although the designed ligands were always better than the marketed drugs in the inhA docking, binding affinities were still higher and more uniformly distributed for DprE1. This reflects inhA's structural heterogeneity and tendency for resistance-associated conformational adjustments, which diminish pocket rigidity and compromise ligand anchoring (Rufa'i et al., 2025).

5.3 DprE1 Is a More Reliable and Druggable Target

Structural evaluation across ten distinct DprE1 conformations revealed a high degree of active-site conservation. Despite minor variations in adjacent loops, the catalytic core and substrate-binding tunnel remained structurally stable and consistently accommodated all five designed ligands (Singh et al., 2022). This stability explains the uniformity of high docking scores and indicates that DprE1 supports recognition of structure-stable inhibitors, a key requirement for robust drug design (Dash et al., 2024). Additionally, the presence of Cys387, a unique nucleophilic hotspot absent in human homologs, enables selective covalent or pseudo-covalent interactions, thereby contributing to exceptionally high binding affinities. Given its essential role in arabinan synthesis and its limited capacity for clinically significant mutations, the data strongly reinforce DprE1's preferential suitability for new anti-TB drug development (Liu et al., 2020).

5.4 InhA Remains Challenging but Viable for Inhibitor Optimization

Although multiple designed ligands showed improved binding compared with marketed drugs, inhA exhibited greater structural variability among the nine conformations evaluated (Nyijime et al., 2025). Minorly shifted residues in the NADH-binding region changed the hydrogen-bond patterns and also the molecular docking scores fluctuated (Terefe & Ghosh, 2022). The differences exemplify experimental data indicating that the process of ligand design for mutant inhA strains to achieve an inhibitory effect is stricter, and that alternative approaches, such as direct covalent warheads, fragment-based design, or multi-target hybrid molecules, might be considered (Sullivan et al., 2006). The uneven binding across the inhA ensemble also underscores the need for resistance-conscious inhibitor design, as conventional ligand scaffolds often lose potency due to subtle structural changes in the drug-binding region (Rizet et al., 2025).

5.5 Strength of Ensemble Docking and Implications for Drug Modeling

A key strength of this study is the combination of ensemble docking across 19 protein structures with a subsequent 100-ns molecular dynamics assessment of the prioritized DprE1–Ligand 5 complex. Ensemble docking captures variation among experimentally determined protein conformations, whereas the MD trajectory provides a time-dependent assessment of structural behavior after docking. The RMSD, Rg, RMSF, and SASA profiles collectively indicate that the simulated complex remained globally stable while retaining localized residue-level flexibility. Thus, the MD analysis adds a dynamic layer of validation to the static docking results rather than relying on ensemble docking alone.

5.6 ADMET Analysis

ADMET study Favorable pharmacokinetic and safety profiles seen in the first ADMET investigation of the created ligands suggested their possible use as drug-like candidates. Most ligands maintained acceptable LogP values, modest polar surface areas, and adherence to Lipinski's rule of five, thereby indicating good oral bioavailability and membrane permeability. Notably, predicted toxicity hazards, including hepatotoxicity and mutagenicity, were low; metabolic stability parameters were compatible with key CYP450 isoforms. Compared with marketed medications, the developed scaffolds exhibited higher drug-likeness indices and balanced absorption–distribution profiles, thereby supporting their suitability for further experimental validation and improvement (Alam et al., 2024).

6. CONCLUSION

This study integrates ensemble molecular docking, ligand design, ADMET prediction, and 100-ns molecular dynamics simulation to investigate DprE1 and InhA as targets for anti-tuberculosis drug discovery. The docking analysis identified DprE1–Ligand 5 as the prioritized complex, with a MolDock score of −983.573 for PDB structure 4FDO. The subsequent 100-ns GROMACS trajectory showed an initial equilibration phase followed by a relatively stable RMSD regime, preservation of overall compactness by Rg, predominantly low residue-level fluctuations with localized flexible regions, and no sustained drift in SASA. These findings provide complementary dynamic support for the structural persistence of the docked DprE1–Ligand 5 complex. However, the results remain computational and should not be interpreted as proof of biochemical inhibition. Independent MD replicates, quantitative free-energy analysis, and experimental enzyme- and whole-cell assays are required to establish the potency and reproducibility of Ligand 5.

7. Future scope

Future work should build on the present 100-ns simulation by performing independent replicate trajectories and, where computational resources permit, longer simulations to test reproducibility of the observed behavior. Protein–ligand hydrogen-bond occupancy, contact persistence, interaction fingerprints, and MM-PBSA/MM-GBSA binding free-energy calculations with residue-wise decomposition could provide a more quantitative assessment of the interactions governing complex stability. Experimental validation should include enzyme inhibition assays and minimum inhibitory concentration (MIC) testing against relevant Mycobacterium tuberculosis strains. Additional studies of cytotoxicity, metabolic stability, permeability, and pharmacokinetics, together with rational ligand optimization, will be necessary before the designed scaffold can be considered for further preclinical development.

DECLARATIONS

Acknowledgment
The authors gratefully acknowledge the Department of Biotechnology, Sri Krishnadevaraya University, Anantapur, Andhra Pradesh, India, and the Indian Biological Sciences and Research Institute (IBRI), Noida, India, for providing the necessary facilities, resources and academic support to carry out this research work.

Ethics Approval and Consent to Participate
Not applicable. This study was entirely computational and did not involve human participants, human specimens, or animal experimentation.

Consent for Publication
Not applicable. This manuscript does not contain any individual person's data or identifiable information.

Competing Interests
The authors declare that they have no competing interests.

Funding
The authors received no specific funding or financial support for this study.

Authors' Contributions
All authors contributed to the conception and design of the study. The computational analyses, molecular docking, ADMET analysis, molecular dynamics simulation, data interpretation, and manuscript preparation were performed by the authors. All authors contributed to the revision of the manuscript and approved the final version for publication.

Availability of Data and Materials
All data generated or analyzed during this study are included in this published article and its supplementary information, where applicable. Additional computational data generated during the study are available from the corresponding author upon reasonable request.

Use of Generative Artificial Intelligence
The authors used ChatGPT (version 5.6) and Grammarly solely for language-related assistance, including improving sentence structure, grammar, readability, and overall English-language clarity. These tools were not used to generate, analyze, or interpret scientific data, to perform computational analyses, or to draw scientific conclusions. The authors remain fully responsible for the scientific content, accuracy, interpretation, and final version of the manuscript.

REFERENCES

1. Abdullahi, S. H., Moin, A. T., Uzairu, A., Umar, A. B., Ibrahim, M. T., Usman, M. T., Nawal, N., Bayil, I., & Zubair, T. (2024). Molecular docking studies of some benzoxazole and benzothiazole derivatives as VEGFR-2 target inhibitors: In silico design, MD simulation, pharmacokinetics and DFT studies. Intelligent Pharmacy, 2(2), 232-250. https://doi.org/https://doi.org/10.1016/j.ipha.2023.11.010
2. Agu, P. C., Afiukwa, C. A., Orji, O. U., Ezeh, E. M., Ofoke, I. H., Ogbu, C. O., Ugwuja, E. I., & Aja, P. M. (2023). Molecular docking as a tool for the discovery of molecular targets of nutraceuticals in diseases management. Sci Rep, 13(1), 13398. https://doi.org/10.1038/s41598-023-40160-2
3. Alam, M., Abbas, K., Raza, M. T., Abedi, S. M. H., Haq, H., & Mustafa, M. (2024). Identification of Aquaporin 3 Inhibitors from Santalum album Phytochemicals for Melanoma treatment: A Computational Study: Targeting Aquaporin 3: Santalum Album in Melanoma Therapy. Iranian Journal of Pharmaceutical Sciences, 20(4), 293- 314. https://doi.org/10.22037/ijps.v20i4.44925
4. Alamri, A., Alafnan, A., Hussein, W. A., Almansour, K., Dhham, A. R., & Abouzied, A. S. (2025). Disrupting tuberculosis pathogenesis by targeting DprE1 in cell wall biosynthesis: a structural dynamics perspective. J Comput Aided Mol Des, 39(1), 45. https://doi.org/10.1007/s10822-025-00626-z
5. Ando, H., Kondo, Y., Suetake, T., Toyota, E., Kato, S., Mori, T., & Kirikae, T. (2010). Identification of katG mutations associated with high-level isoniazid resistance in Mycobacterium tuberculosis. Antimicrob Agents Chemother, 54(5), 1793-1799. https://doi.org/10.1128/aac.01691-09
6. Ansari, M. S., Abbas, K., Alam, M., Usmani, N., Khan, A., Khan, A. A., & Hessini, K. (2025). Investigating the anxiolytic potential of Withania somnifera: a GC–MS and in silico study targeting MAO-A inhibition. Discover Plants, 2(1), 89. https://doi.org/10.1007/s44372-025-00180-w
7. Azram, M., Kaur, M., Rasheed, K., Choudhury, H., Abbas, K., Alam, M., Farheen, A., & Ansari, M. S. (2025). Chronotherapeutic Potential of Withania somnifera Phytocompounds for Narcolepsy Management: An Integrated GC-MS and In Silico Study. Chronobiol Med, 7(3), 177-191. https://doi.org/10.33069/cim.2025.0035
8. Batt, S. M., Jabeen, T., Bhowruth, V., Quill, L., Lund, P. A., Eggeling, L., Alderwick, L. J., Fütterer, K., & Besra, G. S. (2012). Structural basis of inhibition of Mycobacterium tuberculosis DprE1 by benzothiazinone inhibitors. Proc Natl Acad Sci U S A, 109(28), 11354-11359. https://doi.org/10.1073/pnas.1205735109
9. Belete, T. M. (2022). Recent Progress in the Development of Novel Mycobacterium Cell Wall Inhibitor to Combat Drug-Resistant Tuberculosis. Microbiol Insights, 15, 11786361221099878. https://doi.org/10.1177/11786361221099878

10. Bhargava, A., & Bhargava, M. (2020). Tuberculosis deaths are predictable and preventable: Comprehensive assessment and clinical care is the key. J Clin Tuberc Other Mycobact Dis, 19, 100155. https://doi.org/10.1016/j.jctube.2020.100155
11. Biegert, A., & Söding, J. (2009). Sequence context-specific profiles for homology searching. Proc Natl Acad Sci U S A, 106(10), 3770-3775. https://doi.org/10.1073/pnas.0810767106
12. Capela, R., Félix, R., Clariano, M., Nunes, D., Perry, M. J., & Lopes, F. (2023). Target Identification in Anti-Tuberculosis Drug Discovery. Int J Mol Sci, 24(13). https://doi.org/10.3390/ijms241310482
13. Chai, Q., Zhang, Y., & Liu, C. H. (2018). Mycobacterium tuberculosis: An Adaptable Pathogen Associated With Multiple Human Diseases. Front Cell Infect Microbiol, 8, 158. https://doi.org/10.3389/fcimb.2018.00158
14. Chauhan, M., Barot, R., Yadav, R., Joshi, K., Mirza, S., Chikhale, R., Srivastava, V. K., Yadav, M. R., & Murumkar, P. R. (2024). The Mycobacterium tuberculosis Cell Wall: An Alluring Drug Target for Developing Newer Anti-TB Drugs-A Perspective. Chem Biol Drug Des, 104(3), e14612. https://doi.org/10.1111/cbdd.14612
15. Daniel, J., Maamar, H., Deb, C., Sirakova, T. D., & Kolattukudy, P. E. (2011). Mycobacterium tuberculosis uses host triacylglycerol to accumulate lipid droplets and acquires a dormancy-like phenotype in lipid-loaded macrophages. PLoS Pathog, 7(6), e1002093. https://doi.org/10.1371/journal.ppat.1002093
16. Dash, S., Rathi, E., Kumar, A., Chawla, K., & Kini, S. G. (2024). Identification of DprE1 inhibitors for tuberculosis through integrated in-silico approaches. Scientific Reports, 14(1), 11315. https://doi.org/10.1038/s41598-024-61901-x
17. Davoodi, S., Daryaee, F., Iuliano, J. N., Tolentino Collado, J., He, Y., Pollard, A. C., Gil, A. A., Aramini, J. M., & Tonge, P. J. (2023). Evaluating the Impact of the Tyr158 pK(a) on the Mechanism and Inhibition of InhA, the Enoyl-ACP Reductase from Mycobacterium tuberculosis. Biochemistry, 62(12), 1943-1952. https://doi.org/10.1021/acs.biochem.2c00606
18. de Ávila, M. B., Bitencourt-Ferreira, G., & de Azevedo, W. F. (2020). Structural Basis for Inhibition of Enoyl-[Acyl Carrier Protein] Reductase (InhA) from Mycobacterium tuberculosis. Curr Med Chem, 27(5), 745-759. https://doi.org/10.2174/0929867326666181203125229
19. Falzon, D., Schünemann, H. J., Harausz, E., González-Angulo, L., Lienhardt, C., Jaramillo, E., & Weyer, K. (2017). World Health Organization treatment guidelines for drug-resistant tuberculosis, 2016 update. Eur Respir J, 49(3). https://doi.org/10.1183/13993003.02308-2016
20. Friedrich, A., Ripp, R., Garnier, N., Bettler, E., Deléage, G., Poch, O., & Moulinier, L. (2007). Blast sampling for structural and functional analyses. BMC Bioinformatics, 8(1), 62. https://doi.org/10.1186/1471-2105-8-62
21. Grzegorzewicz, A. E., Pham, H., Gundi, V. A., Scherman, M. S., North, E. J., Hess, T., Jones, V., Gruppo, V., Born, S. E., Korduláková, J., Chavadi, S. S., Morisseau, C., Lenaerts, A. J., Lee, R. E., McNeil, M. R., & Jackson, M. (2012). Inhibition of mycolic acid transport across the Mycobacterium tuberculosis plasma membrane. Nat Chem Biol, 8(4), 334-341. https://doi.org/10.1038/nchembio.794
22. Haque, F., Showkat, B., Rasheed, K., Ansari, I., Pawar, V., Alam, M., & Shadab, G. G. H. A. (2025). Identification and Screening of Bioactive Phytocompounds against Matrix Metalloproteinase-9, Targeting Cancer Cell Proliferation and Angiogenesis: Phytocompounds Targeting MMP-9 in Cancer. Iranian Journal of Pharmaceutical Sciences, 21(1), 323-343. https://doi.org/10.22037/ijps.v21i1.48139
23. Hinkson, I. V., Madej, B., & Stahlberg, E. A. (2020). Accelerating Therapeutics for Opportunities in Medicine: A Paradigm Shift in Drug Discovery. Front Pharmacol, 11, 770. https://doi.org/10.3389/fphar.2020.00770
24. Huang, H. J., Lee, K. J., Yu, H. W., Chen, C. Y., Hsu, C. H., Chen, H. Y., Tsai, F. J., & Chen, C. Y. (2010). Structure-based and ligand-based drug design for HER 2 receptor. J Biomol Struct Dyn, 28(1), 23-37. https://doi.org/10.1080/07391102.2010.10507341
25. Hughes, J. P., Rees, S., Kalindjian, S. B., & Philpott, K. L. (2011). Principles of early drug discovery. Br J Pharmacol, 162(6), 1239-1249. https://doi.org/10.1111/j.1476-5381.2010.01127.x
26. Ibrahim, M. A. A., Mahmoud, D. G. M., Abdelrahman, A. H. M., Abdeljawaad, K. A. A., Mekhemer, G. A. H., Shoeib, T., El-Tayeb, M. A., Sidhom, P. A., Paré, P. W., & Hegazy, M.-E. F. (2024). Benzothiazinone analogs as Anti-Mycobacterium tuberculosis DprE1 irreversible inhibitors: Covalent docking, validation, and molecular dynamics simulations. PLOS ONE, 19(11), e0314422. https://doi.org/10.1371/journal.pone.0314422
27. Jacobo-Delgado, Y. M., Rodríguez-Carlos, A., Serrano, C. J., & Rivas-Santiago, B. (2023). Mycobacterium tuberculosis cell-wall and antimicrobial peptides: a mission impossible? Front Immunol, 14, 1194923. https://doi.org/10.3389/fimmu.2023.1194923
28. Johansson, M. U., Zoete, V., Michielin, O., & Guex, N. (2012). Defining and searching for structural motifs using DeepView/Swiss-PdbViewer. BMC Bioinformatics, 13, 173. https://doi.org/10.1186/1471-2105-13-173
29. Kalia, N. P., Hasenoehrl, E. J., Ab Rahman, N. B., Koh, V. H., Ang, M. L. T., Sajorda, D. R., Hards, K., Grüber, G., Alonso, S., Cook, G. M., Berney, M., & Pethe, K. (2017). Exploiting the synthetic lethality between terminal respiratory oxidases to kill Mycobacterium tuberculosis and clear host infection. Proc Natl Acad Sci U S A, 114(28), 7426-7431. https://doi.org/10.1073/pnas.1706139114
30. Kashif, A., Mudassir, A., Mohd Tanjeem, R., Mohd, S., Hisham, A., Farhan, F., Mohd, M., Nazura, U., & Safia, H. (2025). Computational Screening of Natural Compounds Targeting VEGFR-2 for Anti-Angiogenic Therapy. Current Science, Engineering and Technology, 5, 1-27. https://doi.org/http://dx.doi.org/10.2174/0122102981375849250623091708
31. Kashif, A., Raghib, H., Mudassir, A., Abedi, S. M. H., Sana, A., Mohd Wasi, I., Mohd, M., Nazura, U., & Safia, H. (2025). Phytocompounds as Potential EGFR Inhibitors for Glioblastoma Management: A Structure-Based Molecular Docking and Simulation Study. Current Indian Science, 3, 1-17. https://doi.org/http://dx.doi.org/10.2174/012210299X385778250912114718

32. Ke, Q., Gong, X., Liao, S., Duan, C., & Li, L. (2022). Effects of thermostats/barostats on physical properties of liquids by molecular dynamics simulations. Journal of Molecular Liquids, 365, 120116. https://doi.org/https://doi.org/10.1016/j.molliq.2022.120116
33. Kingdon, A. D. H., & Alderwick, L. J. (2021). Structure-based in silico approaches for drug discovery against Mycobacterium tuberculosis. Computational and Structural Biotechnology Journal, 19, 3708-3719. https://doi.org/https://doi.org/10.1016/j.csbj.2021.06.034
34. Lange, C., Dheda, K., Chesov, D., Mandalakas, A. M., Udwadia, Z., & Horsburgh, C. R., Jr. (2019). Management of drug-resistant tuberculosis. Lancet, 394(10202), 953-966. https://doi.org/10.1016/s0140-6736(19)31882-3
35. Lionta, E., Spyrou, G., Vassilatis, D. K., & Cournia, Z. (2014). Structure-based virtual screening for drug discovery: principles, applications and recent advances. Curr Top Med Chem, 14(16), 1923-1938. https://doi.org/10.2174/1568026614666140929124445
36. Liu, L., Kong, C., Fumagalli, M., Savková, K., Xu, Y., Huszár, S., Sammartino, J. C., Fan, D., Chiarelli, L. R., Mikušová, K., Sun, Z., & Qiao, C. (2020). Design, synthesis and evaluation of covalent inhibitors of DprE1 as antitubercular agents. Eur J Med Chem, 208, 112773. https://doi.org/10.1016/j.ejmech.2020.112773
37. Looney, M. M., Lu, Y., Karakousis, P. C., & Halushka, M. K. (2021). Mycobacterium tuberculosis Infection Drives Mitochondria-Biased Dysregulation of Host Transfer RNA-Derived Fragments. J Infect Dis, 223(10), 1796-1805. https://doi.org/10.1093/infdis/jiaa596
38. Mabkhot, Y. N., Alatibi, F., El-Sayed, N. N. E., Al-Showiman, S., Kheder, N. A., Wadood, A., Rauf, A., Bawazeer, S., & Hadda, T. B. (2016). Antimicrobial Activity of Some Novel Armed Thiophene Derivatives and Petra/Osiris/Molinspiration (POM) Analyses. Molecules, 21(2), 222. https://www.mdpi.com/1420-3049/21/2/222
39. Macalino, S. J. Y., Billones, J. B., Organo, V. G., & Carrillo, M. C. O. (2020). In Silico Strategies in Tuberculosis Drug Discovery. Molecules, 25(3). https://doi.org/10.3390/molecules25030665
40. Makarov, V., Manina, G., Mikusova, K., Möllmann, U., Ryabova, O., Saint-Joanis, B., Dhar, N., Pasca, M. R., Buroni, S., Lucarelli, A. P., Milano, A., De Rossi, E., Belanova, M., Bobovska, A., Dianiskova, P., Kordulakova, J., Sala, C., Fullam, E., Schneider, P.,…Cole, S. T. (2009). Benzothiazinones kill Mycobacterium tuberculosis by blocking arabinan synthesis. Science, 324(5928), 801-804. https://doi.org/10.1126/science.1171583
41. Mark, P., & Nilsson, L. (2001). Structure and Dynamics of the TIP3P, SPC, and SPC/E Water Models at 298 K. The Journal of Physical Chemistry A, 105(43), 9954-9960. https://doi.org/10.1021/jp003020w
42. Nyijime, T. A., Shallangwa, G. A., Uzairu, A., Umar, A. B., Ibrahim, M. T., Abdalla, M., Hamadi, A., Barnawi, J., & Madkhali, H. A. (2025). In Silico design and evaluation of novel anti-tubercular agents as Inha inhibitors through a virtual screening approach. Discover Chemistry, 2(1), 299. https://doi.org/10.1007/s44371-025-00367-w
43. Rigby, S. P. (2024). Uses of Molecular Docking Simulations in Elucidating Synergistic, Additive, and/or Multi-Target (SAM) Effects of Herbal Medicines. Molecules, 29(22). https://doi.org/10.3390/molecules29225406
44. Rizet, J., Maveyraud, L., Rengel, D., Guillet, V., Publicola, G., Rodriguez, F., Lherbet, C., & Mourey, L. (2025). Is Mycobacterial InhA a Suitable Target for Rational Drug Design? ChemMedChem, 20(13), e202500079. https://doi.org/10.1002/cmdc.202500079
45. Rufa'i, M. S., Abdulganiyyu, I. A., Ajala, A., Abdalla, M., Alahmadi, R. M., Awadalla, M. E., Abdulganiyyu, K., Mahe, A. u., Gwarzo, Y. S. i., & Kabir, N. (2025). In-silico design and evaluation of quinoline-dione derivatives as Mycobacterium tuberculosis DprE1 inhibitors. Discover Molecules, 2(1), 21. https://doi.org/10.1007/s44345-025-00027-7
46. Salo-Ahen, O. M. H., Alanko, I., Bhadane, R., Bonvin, A. M. J. J., Honorato, R. V., Hossain, S., Juffer, A. H., Kabedev, A., Lahtela-Kakkonen, M., Larsen, A. S., Lescrinier, E., Marimuthu, P., Mirza, M. U., Mustafa, G., Nunes-Alves, A., Pantsar, T., Saadabadi, A., Singaravelu, K., & Vanmeert, M. (2021). Molecular Dynamics Simulations in Drug Discovery and Pharmaceutical Development. Processes, 9(1), 71. https://www.mdpi.com/2227-9717/9/1/71
47. Saritha, K., Alivelu, M., & Mohammad, M. (2024). Drug-likeness analysis, in silico ADMET profiling of compounds in Kedrostis foetidissima (Jacq.) Cogn, and antibacterial activity of the plant extract. In Silico Pharmacol, 12(2), 67. https://doi.org/10.1007/s40203-024-00240-1
48. Sassetti, C. M., & Rubin, E. J. (2003). Genetic requirements for mycobacterial survival during infection. Proc Natl Acad Sci U S A, 100(22), 12989-12994. https://doi.org/10.1073/pnas.2134250100
49. Singh, R., Kumar, S., Bhardwaj, V. K., & Purohit, R. (2022). Screening and reckoning of potential therapeutic agents against DprE1 protein of Mycobacterium tuberculosis. Journal of Molecular Liquids, 358, 119101. https://doi.org/https://doi.org/10.1016/j.molliq.2022.119101
50. Sullivan, T. J., Truglio, J. J., Boyne, M. E., Novichenok, P., Zhang, X., Stratton, C. F., Li, H. J., Kaur, T., Amin, A., Johnson, F., Slayden, R. A., Kisker, C., & Tonge, P. J. (2006). High affinity InhA inhibitors with activity against drug-resistant strains of Mycobacterium tuberculosis. ACS Chem Biol, 1(1), 43-53. https://doi.org/10.1021/cb0500042
51. Terefe, E. M., & Ghosh, A. (2022). Molecular Docking, Validation, Dynamics Simulations, and Pharmacokinetic Prediction of Phytochemicals Isolated From Croton dichogamus Against the HIV-1 Reverse Transcriptase. Bioinform Biol Insights, 16, 11779322221125605. https://doi.org/10.1177/11779322221125605
52. Torktaz, I., Mohamadhashem, F., Esmaeili, A., Behjati, M., & Sharifzadeh, S. (2013). Virtual screening and pharmacophore design for a novel theoretical inhibitor of macrophage stimulating factor as a metastatic agent. Bioimpacts, 3(3), 141-144. https://doi.org/10.5681/bi.2013.026
53. Valafar, S. J. (2021). Systematic Review of Mutations Associated with Isoniazid Resistance Points to Continuing Evolution and Subsequent Evasion of Molecular Detection, and Potential for Emergence of Multidrug Resistance in Clinical Strains of Mycobacterium tuberculosis. Antimicrobial Agents and Chemotherapy, 65(3), 10.1128/aac.02091-02020. https://doi.org/doi:10.1128/aac.02091-20

54. Vanommeslaeghe, K., Hatcher, E., Acharya, C., Kundu, S., Zhong, S., Shim, J., Darian, E., Guvench, O., Lopes, P., Vorobyov, I., & Mackerell, A. D., Jr. (2010). CHARMM general force field: A force field for drug-like molecules compatible with the CHARMM all-atom additive biological force fields. J Comput Chem, 31(4), 671-690. https://doi.org/10.1002/jcc.21367
55. Vázquez, J., López, M., Gibert, E., Herrero, E., & Luque, F. J. (2020). Merging Ligand-Based and Structure-Based Methods in Drug Discovery: An Overview of Combined Virtual Screening Approaches. Molecules, 25(20), 4723. https://www.mdpi.com/1420-3049/25/20/4723
56. Vilchèze, C., & Jacobs, W. R., Jr. (2014). Resistance to Isoniazid and Ethionamide in Mycobacterium tuberculosis: Genes, Mutations, and Causalities. Microbiol Spectr, 2(4), Mgm2-0014-2013. https://doi.org/10.1128/microbiolspec.MGM2-0014-2013
57. Xu, X., Dong, B., Peng, L., Gao, C., He, Z., Wang, C., & Zeng, J. (2022). Anti-tuberculosis drug development via targeting the cell envelope of Mycobacterium tuberculosis. Front Microbiol, 13, 1056608. https://doi.org/10.3389/fmicb.2022.1056608
58. Yadav, S., Soni, A., Tanwar, O., Bhadane, R., Besra, G. S., & Kawathekar, N. (2023). DprE1 Inhibitors: Enduring Aspirations for Future Antituberculosis Drug Discovery. ChemMedChem, 18(16), e202300099. https://doi.org/10.1002/cmdc.202300099
59. Yu, W., & MacKerell, A. D., Jr. (2017). Computer-Aided Drug Design Methods. Methods Mol Biol, 1520, 85-106. https://doi.org/10.1007/978-1-4939-6634-9_5
60. Yushir, M., Soumendranath, B., & Mahmoud, E. S. S. (2015). Computer-aided Identification of Novel DprE1 Inhibitors as Potential Anti-TB Lead Compounds: A Hybrid Virtual-screening and Molecular Dynamics Approach. Letters in Drug Design & Discovery, 12(4), 302-313. https://doi.org/http://dx.doi.org/10.2174/1570180811666141001005536